PolarMatte: Fully Computational Ground-Truth-Quality Alpha Matte Extraction for Images and Video using Polarized Screen Matting

Supplementary Material

A. Derivation of Eq. (6)

Here we derive the relation between the polarimetric triangulation matte α_T and the true alpha matte α described in Eq. (6) from Eq. (4). We first compute the part of $\mathbf{I}_{\phi+\frac{\pi}{2}} - \mathbf{I}_{\phi}$ in Eq. (4) with the polarimetric compositing equation Eq. (5) as follows:

$$\begin{aligned}
&\mathbf{I}_{\phi+\frac{\pi}{2}} - \mathbf{I}_{\phi} \\
&= \alpha\mathbf{P} \odot \left(\cos^2\left(\boldsymbol{\theta}_f - \left(\phi - \frac{\pi}{2}\right)\mathbf{1}\right) - \cos^2\left(\boldsymbol{\theta}_f - \phi\mathbf{1}\right)\right) \\
&\quad + (1-\alpha)\left(\mathbf{B}_{\phi+\frac{\pi}{2}} - \mathbf{B}_{\phi}\right) \\
&= -\alpha\mathbf{P} \odot \cos 2\left(\boldsymbol{\theta}_f - \phi\right) + (1-\alpha)\left(\mathbf{B}_{\phi+\frac{\pi}{2}} - \mathbf{B}_{\phi}\right).
\end{aligned} \tag{28}$$

By substituting this into Eq. (4), we obtain Eq. (6).

B. Derivation of Eq. (27)

Here we derive the solution for PolarIC in Eq. (27) from the objective in Eq. (26). The objective is a least squares problem with a linear equality constraint. We solve this problem using the Lagrange multiplier λ, hence, the objective function can be described as follows:

$$L = \|\mathbf{1} - \mathbf{c}\|_2^2 + \lambda\mathbf{m}^\top\mathbf{c}. \tag{29}$$

The partial derivatives of this objective function with respect to $\mathbf{c}$ and λ are as follows:

$$\frac{\partial L}{\partial \mathbf{c}} = 2\left(\mathbf{c} - \mathbf{1}\right) + \lambda\mathbf{m}, \tag{30}$$

$$\frac{\partial L}{\partial \lambda} = \mathbf{m}^\top\mathbf{c}. \tag{31}$$

Equating these to zero, we obtain the following linear system:

$$\begin{bmatrix} 2\mathbf{E}_4 & \mathbf{m} \\ \mathbf{m}^\top & 0 \end{bmatrix}\begin{bmatrix} \mathbf{c} \\ \lambda \end{bmatrix} = 2\begin{bmatrix} \mathbf{1} \\ 0 \end{bmatrix}. \tag{32}$$

We naïvely calculate the inverse of the matrix on the left-hand side and obtain the solution for $\mathbf{c}$ described in Eq. (27).

C. Local Linear Model for Polarimetric Matting Laplacian

In Sec. 4.2 in the main paper, we used the local linear model:

$$\alpha_i = \mathbf{a}_k^\top\mathbf{s}_i + b_k, \quad \forall i \in \mathcal{W}_k, \tag{33}$$

where α_i and $\mathbf{s}_i \in \mathbb{R}^3$ are the alpha matte and the vector $\mathbf{s}$ of the i-th pixel in a local window $\mathcal{W}_k$. The coefficient vector $\mathbf{a}_k \in \mathbb{R}^3$ and bias $b_k \in \mathbb{R}$ are constant over the local window. This local linear model assumes that the foreground and background Stokes parameters in a local window lie in a low-dimensional space, *e.g.*, their color satisfies the color line model, and phase angles are uniform.

With the definition of the vector $\mathbf{s}$ and Eqs. (8) and (9), the vector $\mathbf{s}$ can be written as follows:

$$\begin{aligned}
\mathbf{s} &= \begin{bmatrix} \mathbf{s}_1 \\ \mathbf{s}_2 \end{bmatrix} \\
&= \alpha \underbrace{\begin{bmatrix} \cos\theta_f & 0 & 0 \\ 0 & \cos\theta_f & 0 \\ 0 & 0 & \cos\theta_f \\ \sin\theta_f & 0 & 0 \\ 0 & \sin\theta_f & 0 \\ 0 & 0 & \sin\theta_f \end{bmatrix}}_{\mathbf{R}}\mathbf{P} \\
&\quad + (1-\alpha)\underbrace{\begin{bmatrix} \cos\theta_b & 0 & 0 \\ 0 & \cos\theta_b & 0 \\ 0 & 0 & \cos\theta_b \\ \sin\theta_b & 0 & 0 \\ 0 & \sin\theta_b & 0 \\ 0 & 0 & \sin\theta_b \end{bmatrix}}_{\mathbf{T}}\mathbf{Q}.
\end{aligned} \tag{34}$$

Here assuming the color line model on the foreground and background color vectors in a local window, *i.e.*, $\mathbf{P} = \beta\mathbf{p}_1 + (1-\beta)\,\mathbf{p}_2$ and $\mathbf{Q} = \gamma\mathbf{q}_1 + (1-\gamma)\,\mathbf{q}_2$, we can rewrite the vector $\mathbf{s}$ as follows:

$$\begin{aligned}
\mathbf{s} &= \alpha\mathbf{R}\left(\beta\mathbf{p}_1 + (1-\beta)\,\mathbf{p}_2\right) \\
&\quad + (1-\alpha)\,\mathbf{T}\left(\gamma\mathbf{q}_1 + (1-\gamma)\,\mathbf{q}_2\right) \\
&= \alpha\left(\mathbf{R}\mathbf{p}_2 - \mathbf{T}\mathbf{q}_2\right) + \alpha\beta\mathbf{R}\left(\mathbf{p}_1 - \mathbf{p}_2\right) \\
&\quad + (1-\alpha)\,\gamma\mathbf{T}\left(\mathbf{q}_1 - \mathbf{q}_2\right) + \mathbf{T}\mathbf{q}_2.
\end{aligned} \tag{35}$$

This equation is transformed into matrix form,

$$\mathbf{s} - \mathbf{T}\mathbf{q}_2 = \underbrace{\begin{bmatrix} \mathbf{R}\mathbf{p}_2 - \mathbf{T}\mathbf{q}_2 & \mathbf{R}\left(\mathbf{p}_1 - \mathbf{p}_2\right) & \mathbf{T}\left(\mathbf{q}_1 - \mathbf{q}_2\right) \end{bmatrix}}_{\mathbf{U}}\begin{bmatrix} \alpha \\ \alpha\beta \\ (1-\alpha)\,\gamma \end{bmatrix}, \tag{36}$$

and α can be described by the multiplication of the first row of the inverse of $\mathbf{U}$ and $\mathbf{s} - \mathbf{T}\mathbf{q}_2$. The basis vectors of the color line models $\mathbf{p}_1$, $\mathbf{p}_2$, $\mathbf{q}_1$, and $\mathbf{q}_2$ are constant over a local window. Therefore, if we assume that the phase angles of the foreground and background, θ_f and θ_b, are constant over a local window, the matrix $\mathbf{U}$ is constant over the local window. Hence, the alpha matte α can be described in

Eq. (33), where $\mathbf{a}_k$ is the first row of the inverse of $\mathbf{U}$, and b_k is the multiplication of the first row of the inverse of $\mathbf{U}$ and $\mathbf{T}\mathbf{q}_2$.

D. Foreground Color Extraction

A straightforward way to extract the foreground color is computing

$$\alpha \mathbf{f}_0 = \mathbf{s}_0 - (1-\alpha)\,\mathbf{b}_0, \tag{37}$$

which is equivalent to the foreground color extraction in an ordinary color image. Since we use polarization, we can also extract the foreground color in the unpolarized domain, *i.e.*, $\alpha\mathbf{F}$. The unpolarized foreground color can be computed as

$$2\alpha\mathbf{F} = \mathbf{s}_0 - \sqrt{\mathbf{s}_1^2 + \mathbf{s}_2^2} - (1-\alpha)\left(\mathbf{b}_0 - \sqrt{\mathbf{b}_1^2 + \mathbf{b}_2^2}\right). \tag{38}$$

When the extracted alpha matte value is close to the true alpha matte, both equations correctly extract the foreground color. However, when the extracted alpha matte value is deviated from the true alpha matte, Eq. (37) yields incorrect foreground color since $\mathbf{b}_0 \gg \mathbf{0}$. In contrast, Eq. (38) is robust to the perturbation of the extracted alpha matte value because we assume almost fully polarized background, and $2\mathbf{B} = \mathbf{b}_0 - \sqrt{\mathbf{b}_1^2 + \mathbf{b}_2^2} \approx \mathbf{0}$. Additionally, unpolarized foreground color extraction can concurrently eliminate the specular reflection component in the foreground color.

E. Details of Test Data Collection

We collected 12 static scene test data for quantitative evaluation. Each scene contains four polarization images of the foreground subject, four background polarization images, foreground subject against blue, white, and black backgrounds, the baseline alpha matte computed by the triangulation matting method [25], and variances of $\mathbf{b}_1$ and $\mathbf{b}_2$. All the images except for the variances are shown in Figs. 9 and 10.

We captured 30 background polarization images, placed a foreground subject, and captured 30 polarization images against the blue, white, and black backgrounds, separately. The polarization images of the foreground subject is one frame randomly selected from 30 polarization images with the white background. The background polarization images are the frame-wise average of the 30 background polarization images. The image with blue background is $\mathbf{s}_0$ of one frame randomly selected from 30 frames captured with the blue background. The images with white and black backgrounds are computed by taking frame-wise averages of $\mathbf{s}_0$ of 30 frames, respectively, which are used to compute the baseline alpha matte by triangulation matting.

F. Effect of PolarIC on DoP and AoP

The proposed PolarIC minimally adjusts the polarization image intensities to satisfy the physical contraint. The experimental results show a favorable affect on matting quality; however, it may unfavorably affect DoP and AoP. Therefore, we computed the average and standard deviation of the difference in the DoP and AoP before and after PolarIC on the static scene test data. The results were $1.12 \times 10^{-2} \pm 6.12 \times 10^{-2}$ and $0.32^\circ \pm 3.02^\circ$, respectively, which suggests that the DoP and AoP are well preserved after PolarIC.

G. Additional Results on Static Scene Test Data

Figures 11 and 12 show additional visual results on static scene test data, where we show the baseline alpha matte computed by triangulation matting (TM), alpha mattes estimated by polarimetric triangulation matting (PTM), background matting (BGM), Keylight, and our PolarMatte method. The color map in the right most column indicates how the alpha matte values are estimated. The blue, green, and red colors indicate pixels estimated by the robust least squares solution, phase angle thresholding, and total optimization, respectively.

H. Additional Results on Dynamic Scenes

Figure 13 shows additional visual results on dynamic scenes, where we show alpha mattes estimated by polarimetric triangulation matting (PTM), background matting (BGM), Keylight, and our PolarMatte method.

We show the video results in the supplementary video. We highly recommend watching the video to evaluate the matting ability of our method for dynamic scenes.

I. Additional Matting Laplacian Comparison

Figures 14 and 15 show additional spectral analysis of our polarimetric matting Laplacian and the original matting Laplacian [10] on the static scene test data.

J. Three-Channel Alpha Matting

Our PolarMatte method is monochromatic, which implicitly assumes that the opacity of an object is constant across each color channel. However, if the foreground subject has colored transparency, the estimated alpha matte by our method may incorrectly average the true alpha matte values across color channels. Here we examine the applicability of our method to three-channel alpha matting by applying our method to each color channel independently.

Figure 16 shows the estimated three-channel and single-channel alpha mattes and images composited with the al-

pha mattes. Our method estimates the reasonably accurate single-channel alpha mattes for the colorful transparent bottles. However, the image composited with the single-channel alpha matte suggests a limitation in reproducing the vibrancy of colorful transparent objects. In contrast, the results show the ability of our method to estimate a three-channel alpha matte, which correctly reproduces the vibrancy of colorful transparent objects in the composite image.

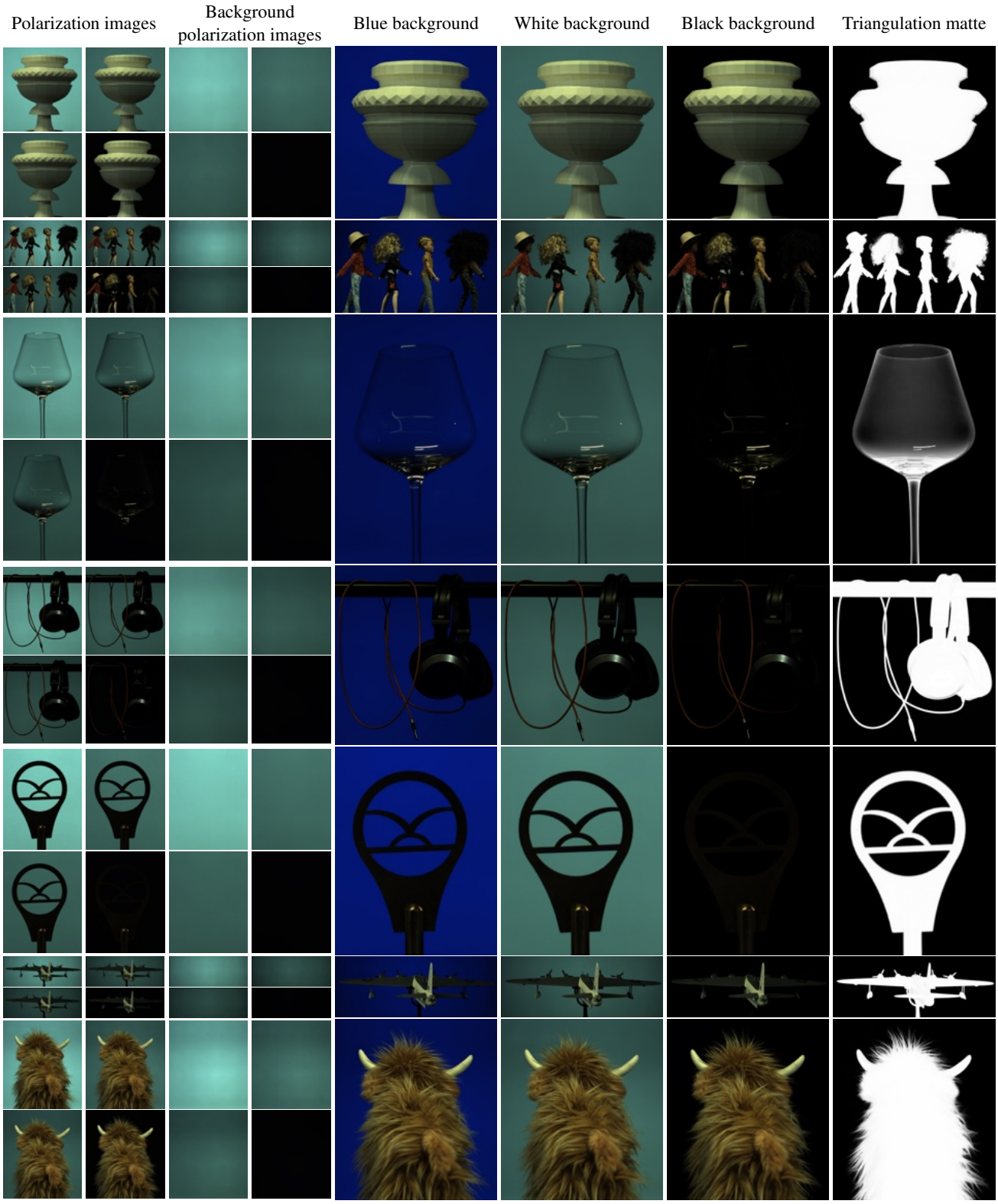

Figure 9. Seven in-focus static scenes out of the twelve test data we collected for quantitative evaluations.

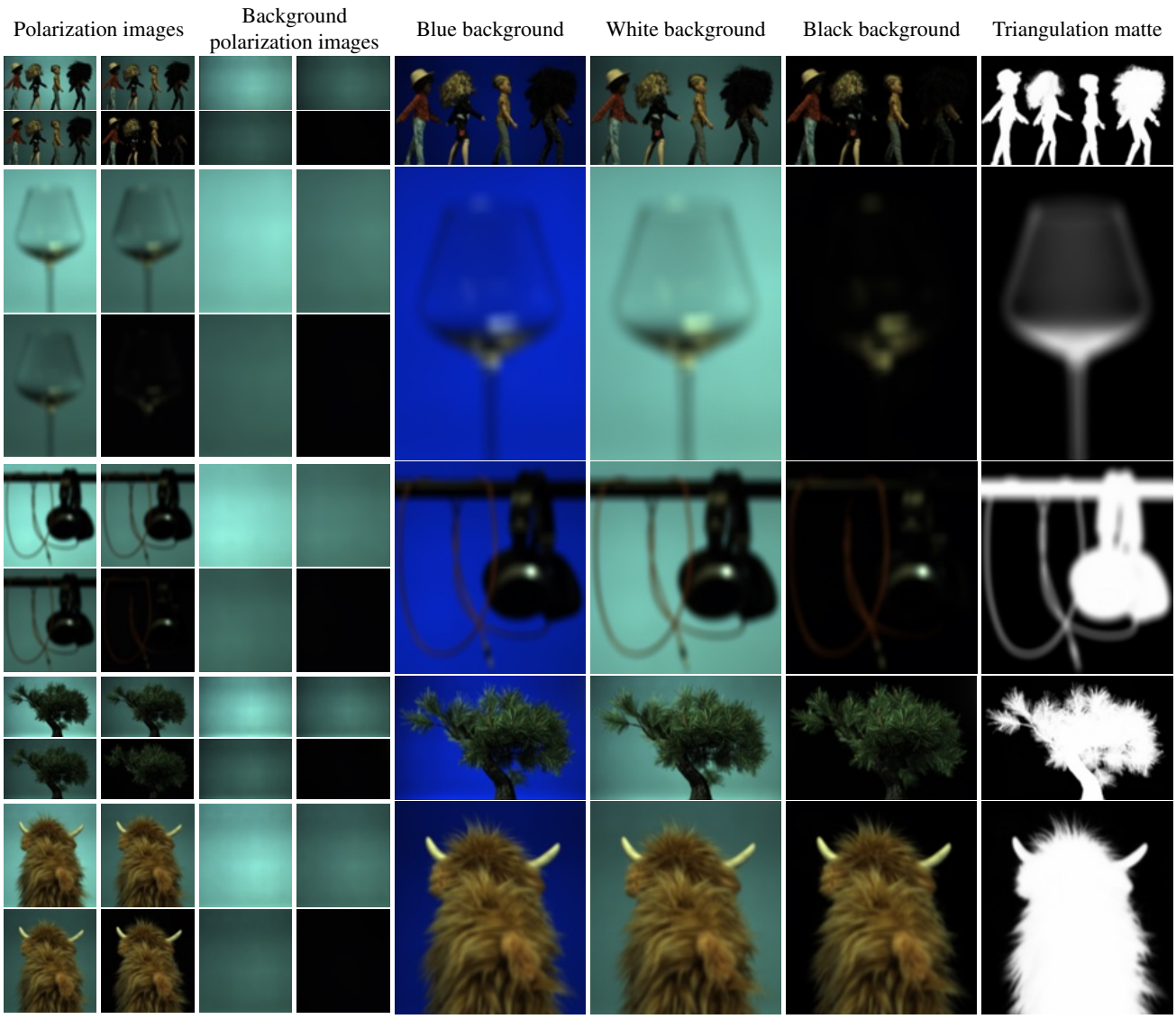

Figure 10. Five out-of-focus static scenes out of the twelve test data we collected for quantitative evaluations.

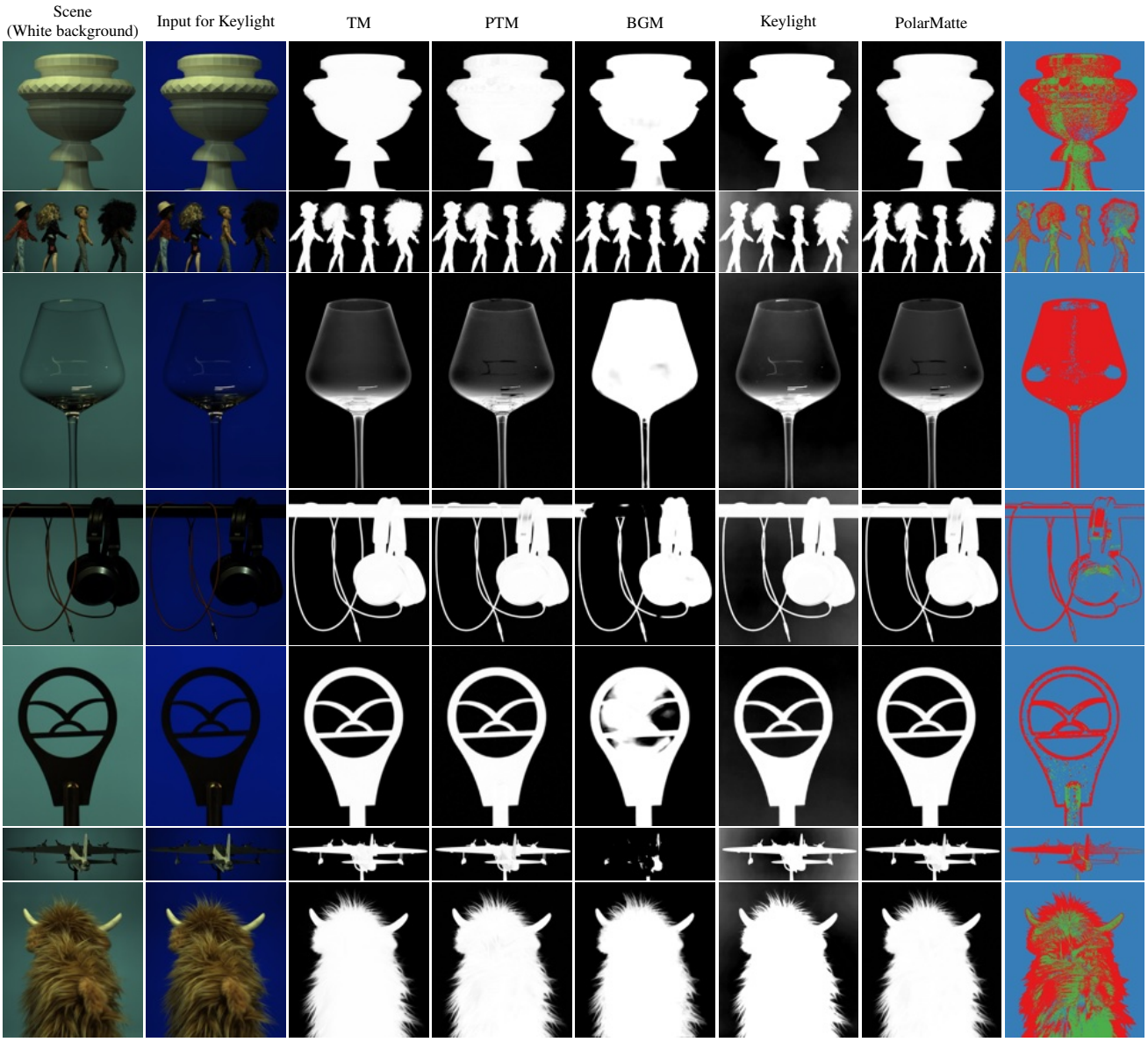

Figure 11. Additional visual results on static scene test data part (1). We show the baseline alpha matte computed by triangulation matting (TM), alpha mattes estimated by polarimetric triangulation matting (PTM), background matting (BGM), Keylight, and our PolarMatte method. The color map in a right most column indicates how the alpha matte values are estimated. The blue, green, and red colors indicate pixels estimated by the robust least squares solution, phase angle thresholding, and total optimization, respectively.

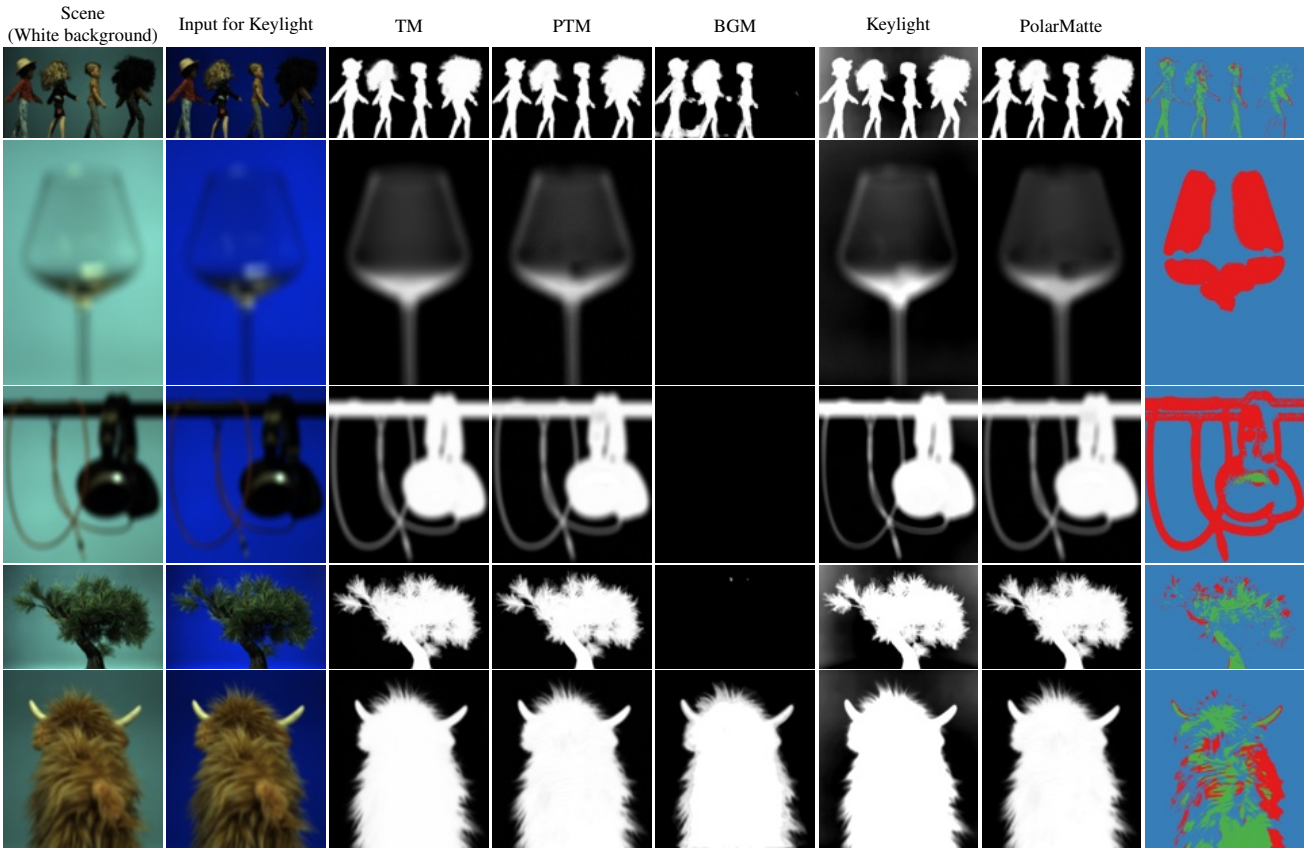

Figure 12. Additional visual results on static scene test data part (2). See explanations in the caption of Fig. 11.

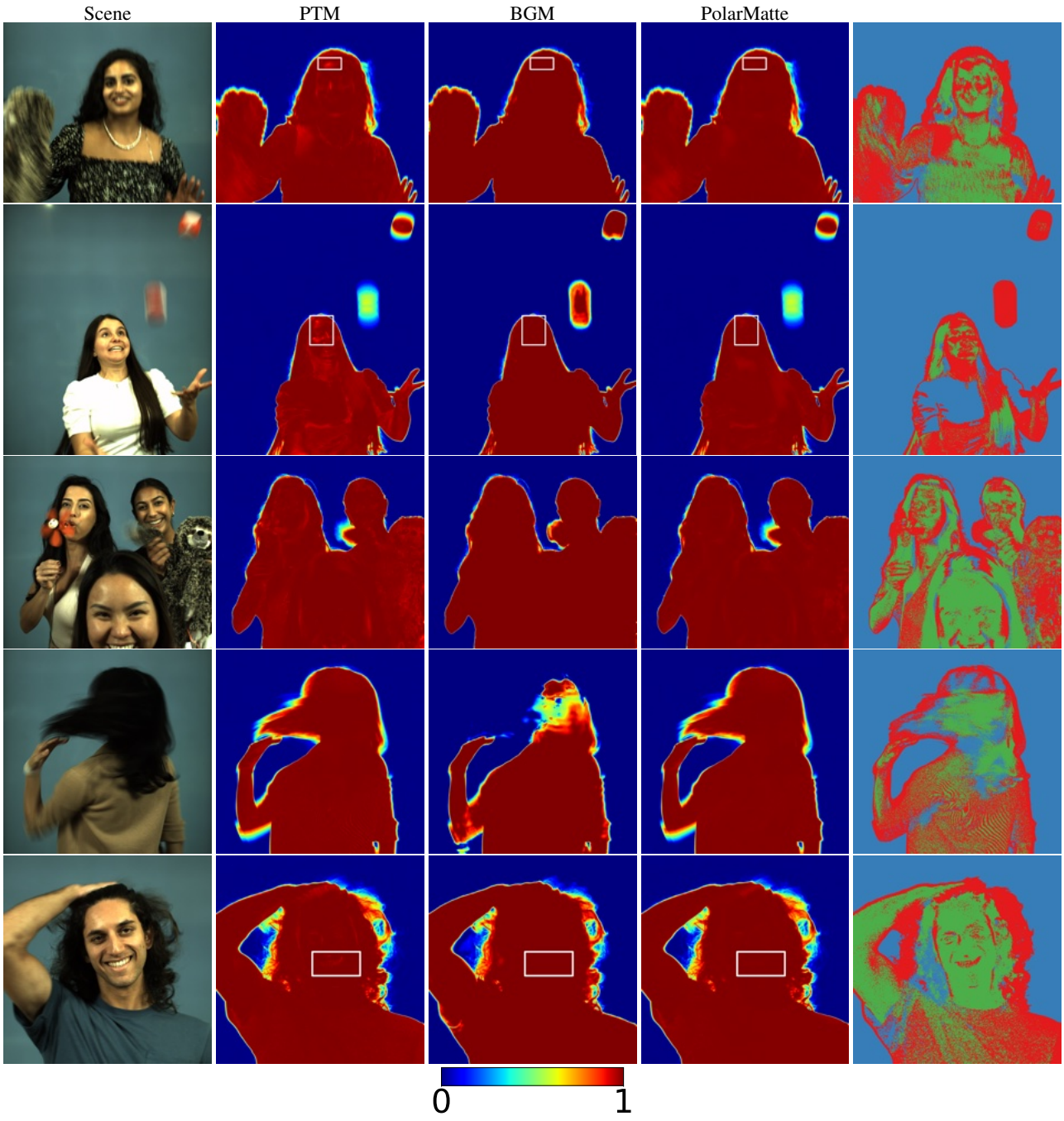

Figure 13. Additional visual results on dynamic scenes. We show the alpha mattes estimated by polarimetric triangulation matting (PTM), background matting (BGM), and our PolarMatte method, visualized using a color gradient encoding to emphasize smaller differences. White rectangles draw attention to interior regions where PTM is overly transparent despite the object being opaque - this effect is significantly reduced using PolarMatte. The color map, in the right-most column, indicates how the alpha matte values are estimated. The blue, green, and red colors indicate pixels estimated by the robust least squares solution, phase angle thresholding, and total optimization, respectively.

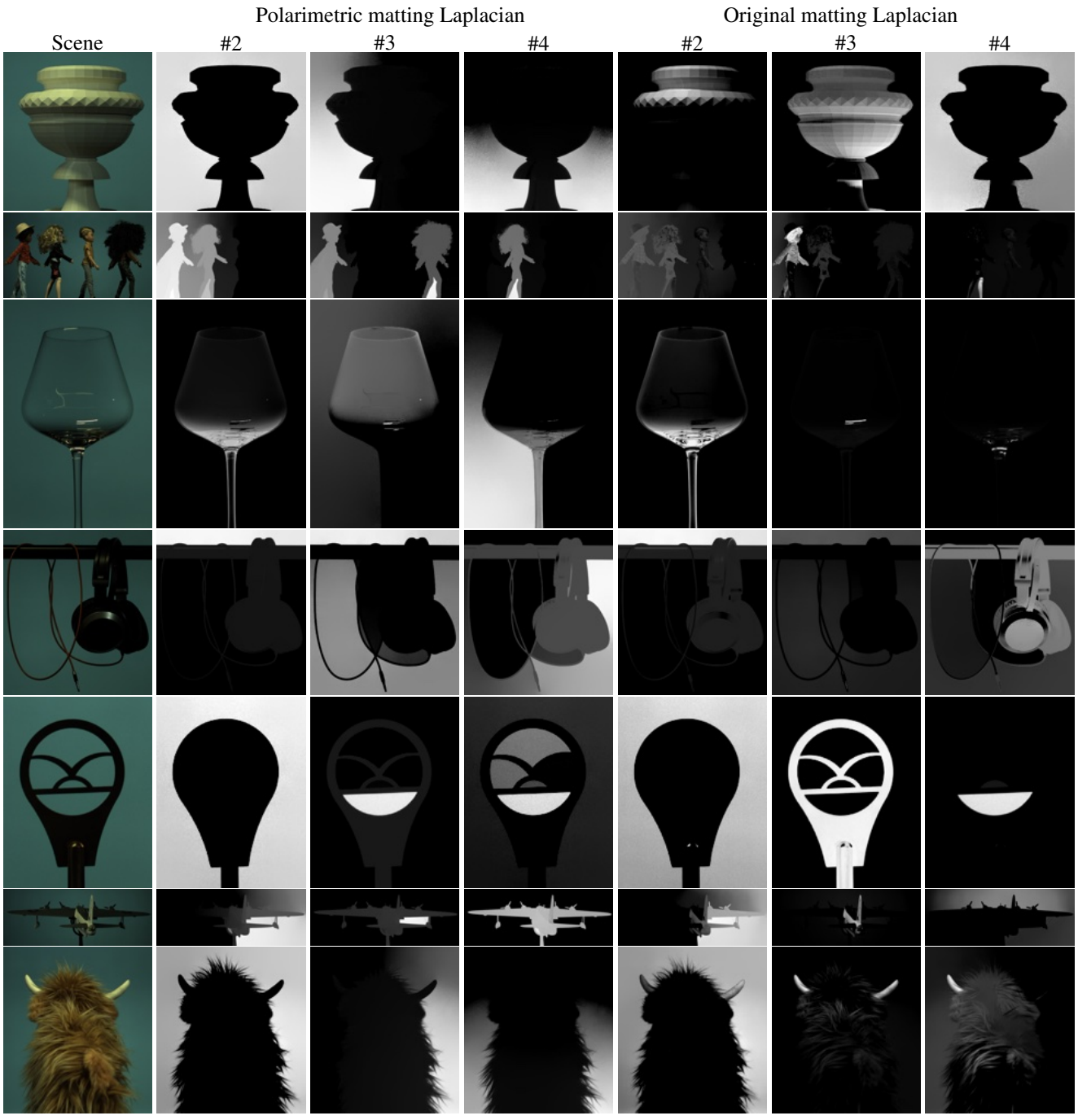

Figure 14. Additional spectral analysis of our polarimetric matting Laplacian and the original matting Laplacian [10] part (1). Figures show the second, third, and fourth smallest eigenvectors of each matting Laplacian (the first smallest eigenvector is constant for both matrices).

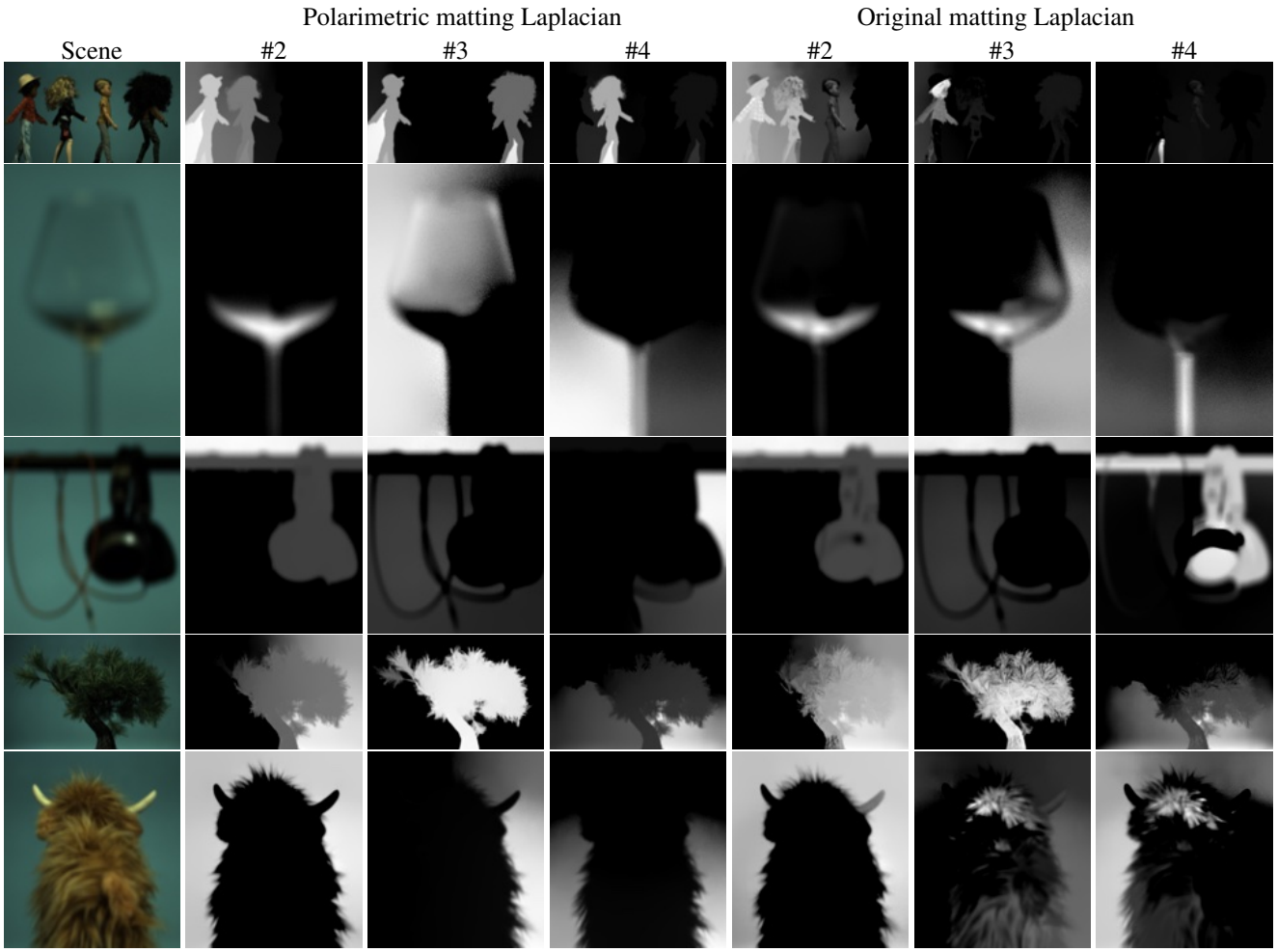

Figure 15. Additional spectral analysis of our polarimetric matting Laplacian and the original matting Laplacian [10] part (2). See explanations in the caption of Fig. 14.

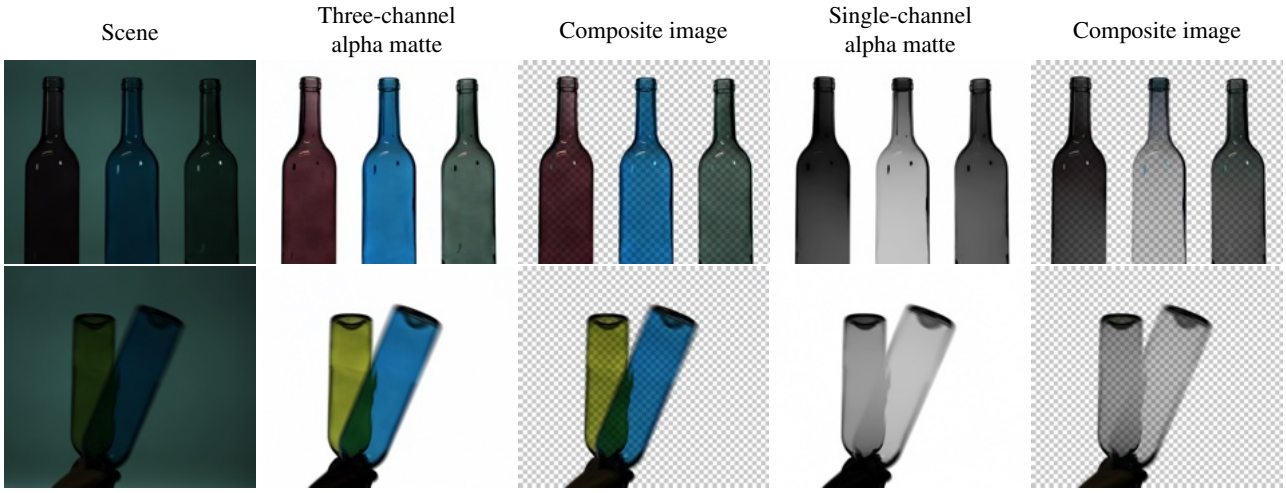

Figure 16. Estimated three-channel and single-channel alpha mattes and images composited with those alpha mattes. We show $1 - \alpha$ instead of α for the three-color alpha matte to match its color to the color of the observed image.